TELKOMNIKA Telecommunication, Computing, Electronics and Control
Vol. 18, No. 4, August 2020, pp. 1719~1730
ISSN: 1693-6930, accredited First Grade by Kemenristekdikti, Decree No: 21/E/KPT/2018
DOI: 10.12928/TELKOMNIKA.v18i4.14988

Simulation and optimization of a tuneable rectangular microstrip patch antenna based on hybrid metal-graphene and FSS superstrate for fifth-generation applications

Nidal Qasem[1], Hamzah M. Marhoon[2]
[1]Department of Electronics and Communications Engineering, Al-Ahliyya Amman University, Jordan
[2]Department of Computer Techniques Engineering, Al-Esraa University College, Iraq

Article Info

Article history:

Received Dec 13, 2019
Revised Jan 6, 2020
Accepted Jan 19, 2020

Keywords:

5G
60 GHz
FSSs
Graphene
Microstrip patch antenna
Tuneable antenna

ABSTRACT

In this paper, a tuneable rectangular microstrip patch antenna (MPA) is simulated and optimized to operate in four frequency bands of the next generation of wireless communication systems. The proposed design incorporates a copper radiating patch with four implanted graphene strips for tuning purposes. The reconfigurable surface impedance of graphene can easily be altered by applying a DC voltage bias directly to the graphene strips, allowing the operating frequency of the antenna to be tuned as desired. The capability of the applied voltage to tune the operating frequency band of the proposed antenna is studied via computer simulation technology (CST) microwave studio (MWS). Frequency selective surfaces (FSSs) are introduced in order to improve the radiation parameters of the antenna. The operating frequency band of the tuneable rectangular MPA increases directly as the applied DC voltage bias is increased. Based on the simulation results, a tuneable rectangular MPA placed between two FSSs is proposed for fifth-generation applications.

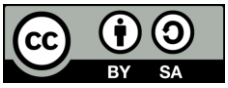

Corresponding Author:

Nidal Qasem,
Department of Electronics and Communications Engineering, Faculty of Engineering,
Al-Ahliyya Amman University,
Zip-code (Postal Address): 19328, Amman, Jordan.
Email: Ne.qasem@ammanu.edu.jo

1. INTRODUCTION

Enormous developments in communication technology, especially in wireless communication, have taken place in recent decades. With these changes in mind, the network operators have introduced advanced generations from time to time. Following the first-generation mobile network in the 1980s, the second generation appeared in the 1990s, the third in 2001, and the fourth in 2010. The next target is the implementation of the fifth-generation network, which is expected to begin in 2020 [1]. With the increase in network applications and demand for higher data rates, switching to higher frequencies is the only option for avoiding data congestion that remains to wireless technology operators. Higher frequency bands offer higher data rates together with the spectral efficiency that is currently required. It is expected to reach real gigabytes bitrate in the millimetre-wave (mm-wave) spectrum in a range between 30 and 300 GHz. In the mm-wave range, the prospect of using the unlicensed frequency band from 57 to 64 GHz for Industrial, Scientific, and Medical (ISM) applications is promising [2, 3].

This frequency band has attracted increased interest and attention in the research community because of its possible practical advantages for future applications. The creation of new technologies in this frequency

band has resulted in many high-speed wireless innovations, including high-definition video streaming, high-speed internet, high-definition multimedia interfaces, wireless gigabit Ethernet, and automotive radar [4].

The primary challenge in the mm-wave regime is increased path losses, which mean that the signal is easily attenuated; the signal may also fade during rainfall. Therefore, mm-waves are preferentially used to provide high data transfer rates in short distance communication. A critical element for such applications is a compact antenna, which should be able to provide reasonable gain, high radiation efficiency, and wide operating frequency bandwidth [5, 6]. Many techniques can be used to achieve tuneable antennas, including radio frequency microelectromechanical system switches, varactor switches, PIN diodes, field effect transistor switches, light-activated switches, or tuneable materials, which may be tuned by applying the appropriate light, magnetic, mechanical, thermal, or electrical bias [7].

Graphene, a conjugated carbon sheet structured in a two-dimensional hexagonal lattice, enables multi-functional signal emission, transmission, modulation, and detection by devices that feature high speed, small size, and particularly low loss. Graphene possesses a reconfigurable surface impedance that can be varied by applying a DC voltage bias to the graphene sheet, which can be used as an alternative to electronic components in designing tuneable antennas. An antenna may be tuned by changing its electrical length, which can be accomplished by increasing or decreasing the current distribution over the radiating patch of the antenna. Alternatively, the physical length of the antenna may be increased by adding an additional shape directly coupled with the radiating antenna patch using graphene as a switch to connect or disconnect the extension to the antenna radiating patch. The tuneable antenna is useful for addressing the issue of the narrow bandwidth in microstrip patch antennas (MPAs) [8-10].

Frequency Selective Surfaces (FSSs) are planar periodic structures whose reflection or transmission properties vary with frequency. A frequency selective surface (FSS) element acts as a passive electromagnetic filter that selectively reflects or attenuates the desired frequency band. The FSS structure exhibits a high surface impedance that reflects plane waves in phase and suppresses surface waves. Integrating an FSS with a rectangular microstrip patch antenna (MPA) can enhance radiation efficiency, bandwidth, and gain while reducing side and back lobes in the radiation pattern [11, 12].

In this work, a design is proposed for a tuneable rectangular MPA with sufficient reconfigurability range to compensate for the narrow bandwidth of MPAs. Since mm-wave antennas composed entirely of graphene are expected to have low antenna performance and a small reconfigurability range, the proposed design uses a hybrid of copper and graphene to achieve reasonable antenna efficiency and gain as well as an acceptable tuneable frequency range. The design is simulated and optimized for fifth-generation applications. The paper is organised as follows: section 2 presents the simulation procedure for the rectangular MPA, using MATLAB to obtain the antenna dimensions and computer simulation technology (CST) microwave studio (MWS) to simulate the rectangular MPA. Section 3 presents the simulation and modelling procedure for the proposed design of the tuneable rectangular MPA. In Section 4, the FSS superstrate layers are used to enhance the tuneable rectangular MPA gain, return loss, and bandwidth of the tuneable rectangular MPA. A discussion of the simulation results obtained from the time domain solver of CST-MWS is given in section 5. Finally, section 6 presents the conclusions of the work.

2. ANTENNA SIMULATION MODELLING

The design procedure for the proposed tunable antenna is shown in Figure 1. In designing the rectangular MPA, three key parameters must be selected: the resonant frequency (f_r), the relative permittivity (ε_r), and the substrate height (h). Table 1 displays the fundamental parameters chosen for this design.

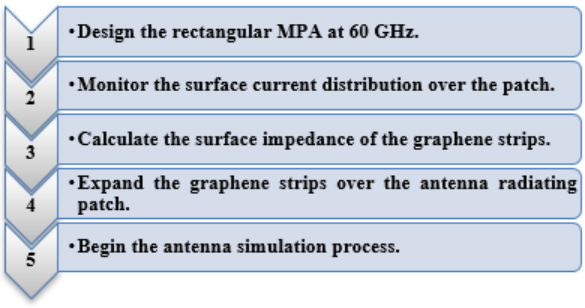

Figure 1. The block diagram of the proposed tuneable rectangular MPA design

Table 1. Fundamental antenna parameters

Parameter	Value
Operating frequency (f_r)	60 GHz
Substrate relative permittivity (ε_r)	2.1
Substrate height (h)	0.1 mm
Input impedance (R_{in})	50 Ω

The MPA can be powered using different methods, such as a coaxial probe, a microstrip line feeding technique, or aperture or proximity coupling methods. In this work, the inset feeding technique is used in order to obtain the optimal impedance between the antenna and the source of the electrical wave. The input impedance of the inset-fed rectangular MPA depends on the feed inset (f_i) inside the patch and, to a certain degree, on the gap between the feed line and the patch (G_{pf}). In the inset feeding method, the resonance frequency shifts with variations in G_{pf} and the return loss of the antenna changes as f_i is varied [13]. Table 2 shows the dimensions of the ground plane, substrate, patch, and feed line of the simulated antenna, which were calculated using the following equations [14, 15]:

$$W = \frac{c}{2f_r\sqrt{\frac{(\varepsilon_r+1)}{2}}} \tag{1}$$

$$\varepsilon_{reff} = \frac{\varepsilon_r+1}{2} + \frac{\varepsilon_r-1}{2}\left[1+12\frac{h}{W}\right]^{\frac{-1}{2}} \tag{2}$$

$$\Delta L = 0.412h\frac{(\varepsilon_{reff}+0.3)\left[\frac{W}{h}+0.264\right]}{(\varepsilon_{reff}-0.258)\left[\frac{W}{h}+0.8\right]} \tag{3}$$

$$L_{eff} = \frac{c}{2f_r\sqrt{\varepsilon_{reff}}} \tag{4}$$

$$L = L_{eff} - 2\Delta L \tag{5}$$

$$f_i = \frac{\cos^{-1}\left(\sqrt{\frac{Z_f}{R_{in}}}\right)}{\frac{\pi}{L}} \tag{6}$$

$$B = \frac{377\pi}{2Z_f\sqrt{\varepsilon_r}} \tag{7}$$

$$W_f = \frac{2h}{\pi}\left\{B-1-\ln(2B-1)+\frac{\varepsilon_r-1}{2\varepsilon_r}\left[\ln(B-1)+0.39-\left(\frac{0.61}{\varepsilon_r}\right)\right]\right\} \tag{8}$$

$$L_f = 3.96 \times W_f \tag{9}$$

$$G_{pf} = \frac{c\times 4.65\times 10^{-9}}{f_r\sqrt{2\varepsilon_{reff}}} \tag{10}$$

$$W_s = 2 \times W \tag{11}$$

$$L_s = 2 \times L, \tag{12}$$

where ε_{reff} is the effective relative permittivity, h is the height of the dielectric substrate, W is the width of the patch, L_{eff} is the effective patch length, L is the actual patch length, ΔL is the length extension, Z_f is the equivalent feed line impedance which is 50 Ω , R_{in} is the resonant input resistance when the patch is fed at the radiating edge, W_f is the feed line width, L_f is the feed line length, W_S is the substrate width, and L_S is the substrate length. The dimensions of the patch, substrate, and feed line are illustrated in Figure 2. The parameters calculated from the previous equations were implemented in CST-MWS to simulate the antenna. Figure 3 illustrates the rectangular MPA in the CST-MWS simulation software.

The optimisation procedure involves minimising or maximising certain antenna dimensions and other parameters, such as the substrate thickness or the relative permittivity. Here, the goals of the optimisation are

to improve the bandwidth, return loss, and impedance matching, as well as, to facilitate the antenna fabrication process where the laser machining accuracy in manufacturing the antenna is 0.08 mm [10]. After the rectangular MPA design was completed, the optimisation procedure was carried out using trial and error. Table 3 presents the optimised parameters for a rectangular MPA.

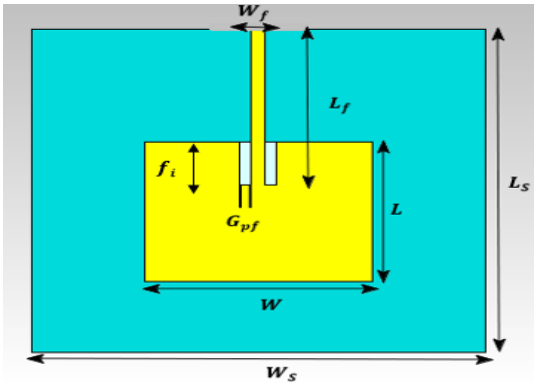

Figure 2. Dimensions of the single rectangular MPA and feed line

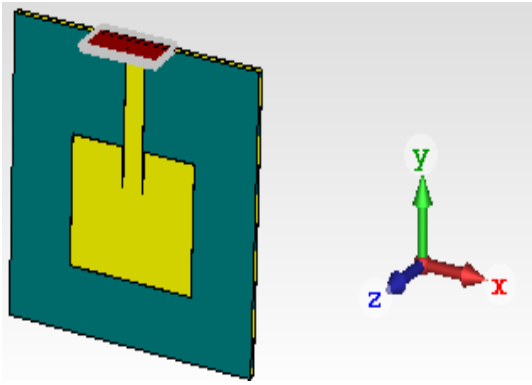

Figure 3. Simulated rectangular MPA in CST-MWS

Table 2. Calculated antenna parameters

Parameter	Value (mm)
Patch width (W)	2.008
Patch length (L)	1.6681
Substrate width (W_S)	4.016
Substrate length (L_S)	3.3362
Feed line inset (f_i)	0.58217
Feed line width (W_f)	0.308
Feed line length (L_f)	1.21968
Gap between the feed line and the patch (G_{pf})	0.0179

Table 3. Optimised rectangular MPA dimensions

Parameter	Value (mm)
Patch width (W)	2
Patch length (L)	1.625
Substrate width (W_S)	4
Substrate length (L_S)	3.25
Feed line inset (f_i)	0.5
Feed line width (W_f)	0.12
Feed line length (L_f)	1.8
Gap between the feed line and the patch (G_{pf})	0.1

3. GRAPHENE-BASED TUNEABLE RECTANGULAR MPA

The rectangular hybrid graphene-metal MPA studied in this work is comprised of a copper radiating patch, in which four strips of graphene are implanted, and a solid copper ground plane. The second key step in the design of the tuneable MPA is the positioning of the graphene strips over the radiating patch. The ideal location depends on the current distribution over the patch, where the graphene strips are inserted in the good accumulated current position. Figure 4 illustrates the surface current distribution over the radiating patch of the rectangular MPA at the operating frequency.

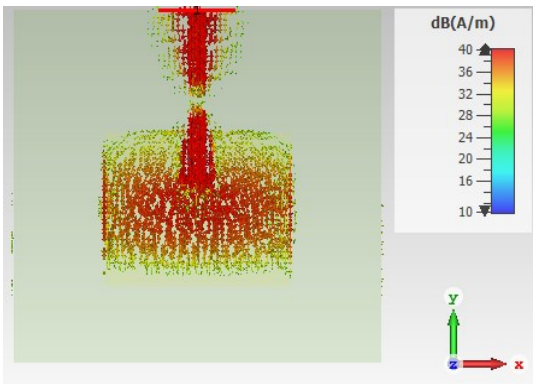

Figure 4. Surface current distribution over the radiating patch

The graphene strips serve as a controlled switch to direct the current flow over the surface of the antenna radiating patch. The effective length of the radiating patch then depends on the DC voltage bias (V_B): in the ON state it remains constant, while in the OFF state the effective length is shorter than the actual length. The ON state corresponds to a low graphene surface impedance, which allows the current to flow through the strip, whereas the OFF state corresponds to a high surface impedance, preventing the flow of the current through the strip. The ON/OFF state is determined by the V_B across the graphene strips. V_B could be applied directly through the feed port if the same voltage is given to all the graphene strips so that they are all activated/deactivated at the same time. Practically, V_B can be input using a broadband commercial bias tee, which is connected between the port of a vector network analyzer and the antenna input microstrip line. The V_B is then applied between the antenna ground plane and the graphene strips inside the antenna radiating patch [16]. In order to obtain the practical values for the ON and OFF surface impedances ($Z_{s_{ON}}$ and $Z_{s_{OFF}}$), the following equations are used [17-19]:

$$n = \frac{\varepsilon_o \varepsilon_r V_B}{dq} \tag{13}$$

$$\mu_c = \hbar v_f \sqrt{n\pi} \tag{14}$$

$$\tau_s = \frac{4\hbar^2 \rho_m {v_{ph}}^2 v_f}{\sqrt{n\pi} k_B T D^2} \tag{15}$$

$$\tau_l = \frac{\mu_l \hbar \sqrt{n\pi}}{q\, v_f} \tag{16}$$

$$Z_s = \frac{j\pi\hbar^2(2\pi f_r(\tau_l\tau_s) - j(\tau_l+\tau_s))}{q^2(\tau_l\tau_s)\left[\mu_c + 2k_B T \ln\left(e^{-\frac{\mu_c}{k_B T}}+1\right)\right]}, \tag{17}$$

where τ_l is the scattering effect, τ_s is the relaxation time, μ_l is the electron mobility (in m^2/Vs), $\rho_m = 7.6 \times 10^{-7}$ is the two-dimensional mass density of graphene in (in kg/m^2), v_{ph}= 2.1×10^4 m/s is the velocity of longitudinal acoustic phonons in graphene, T is the temperature in Kelvin, $\hbar$ is the reduced Planck's constant, k_B is the Boltzmann constant, q is the electron charge (in C), μ_c is the graphene chemical potential (in eV), v_f =1×10^6 m/s is the Fermi velocity, n is the carrier density (in m^{-2}), d is the graphene thickness (in m), and D is the deformation potential (in eV). From recent experimental studies, D ~18 eV appears to be a prevalent and recognized value for graphene over a substrate [17]. The value of $Z_{s_{ON}}/Z_{s_{OFF}}$ may be determined by increasing/decreasing the charge carrier density according to (13), Table 4 illustrates selected parameter values for the graphene surface impedance modelling in both the ON and OFF states.

Different values of V_B were chosen in order to study the effects of increasing or decreasing V_B on the tuning of the f_r. A large value of V_B mayn't be chosen for applications with low power consumption, such as mobile phones. However, the value of V_B is not universal and can be decreased, depending on the application and the required operating frequency band, by selecting a thin substrate with a greater ε_r. The graphene strips were simulated and modelled in CST-MWS as a thin ohmic sheet surface impedance. Table 5 illustrates the graphene strip dimensions, and Figure 5 shows the simulated antenna in CST-MWS.

In order to demonstrate the activation or deactivation process for the graphene strips to change the f_r, Figure 6 illustrates the surface current distribution over the antenna radiating patch and the graphene strips at 60 GHz. When the graphene strips are in the OFF state, a small current is allowed to propagate along with the strips due to the large value of Z_S, contrary that when the graphene strips are in the ON state, substantially more current is capable to propagate along the strips due to the small value of Z_S.

Table 4. Selected parameter values for the graphene Z_S modelling

Parameter	Value			
State		ON		OFF
μ_l (m^2/Vs).		2.7		2.7
D (eV)		4		4
T (K)		295		295
V_B (V)	5	20	30	0.5
n (m^{-2})	5.8×10^{16}	2.32×10^{17}	3.48×10^{17}	6×10^{14}
Z_S(Ω/)	27.71 +j 9.256	11.4 + j5.7	8.1 + j4.65	2569.6+j74.72

Table 5. Graphene strips dimensions

Strip	Dimension (mm)	Strip	Dimension (mm)
S_1	0.16×0.53	D_1	0.65
S_2	0.16×0.54	D_2	0.35
S_3	0.16×0.54	D_3	0.65
S_4	0.16×0.53	D_4	0.27
D_5	0.35	D_6	0.06
D_7	0.27	D_8	0.05

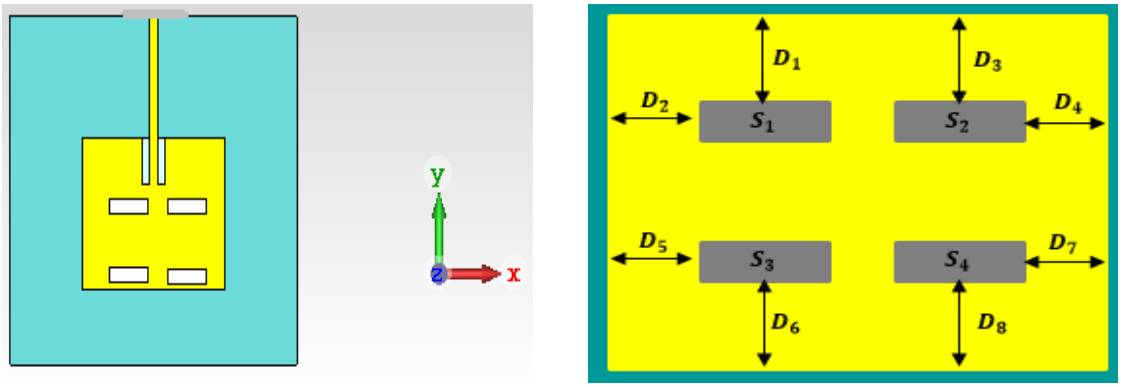

(a) (b)

Figure 5. Tuneable rectangular MPA; (a) Proposed design in CST-MWS and (b) Dimensions of the graphene strips implanted in the radiating patch

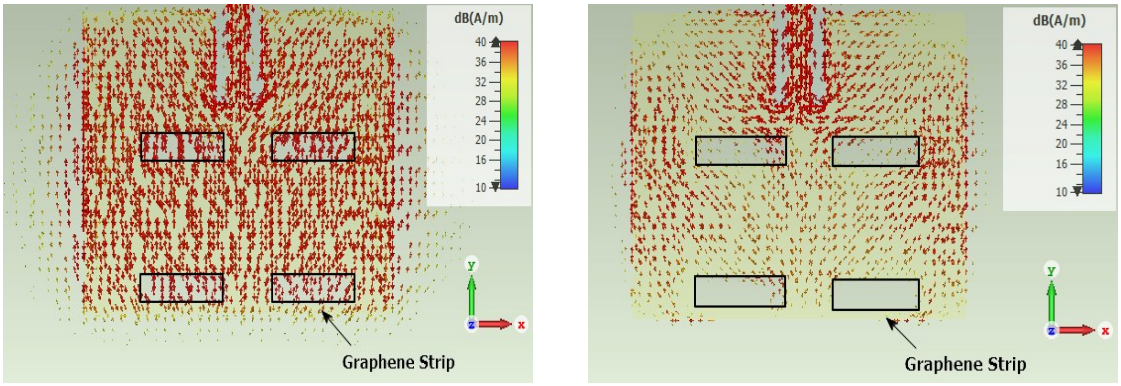

(a) (b)

Figure 6. Surface current distribution over the radiating patch and graphene strips; (a) ON state and (b) OFF state

4. DESIGN OF THE FSS SUPERSTRATE LAYER

To improve the antenna parameters, an FSS superstrate on the top/bottom of the tuneable rectangular MPA, separated by an air gap, is introduced. Using one or more FSS superstrates, various resonance frequencies can be achieved, although there are limitations imposed by the required compact antenna size. It should be noted that an FSS superstrate significantly reduces the impedance bandwidth. The configuration proposed here for a tuneable rectangular MPA integrated with an FSS provides improved performance in multiple parameters, including gain, return loss, and bandwidth, for 60 GHz applications. The FSS is utilised in two ways: as a reflector, formed by a stop-band FSS; and as a superstrate, with a pass-band FSS structure. The proposed FSS is designed to operate in the frequency range 50-70 GHz, with a resonance frequency of 60 GHz. A square loop (SL) element, which has the best performance amongst the simple geometric shapes [20], is chosen for both FSSs. The material used is copper which its thickness is 0.07 mm. The dielectric material is Arlon AD 300 which has 0.1 mm thickness and its relative permittivity is 3. Figure 7 illustrates the geometry of the SL array FSS used in the study.

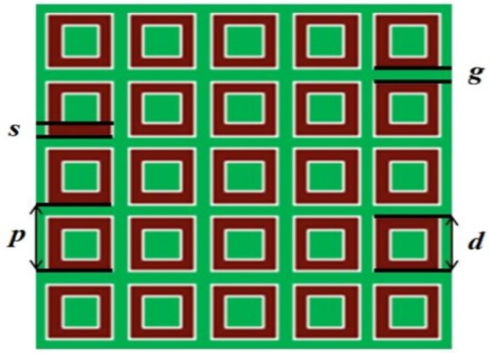

Figure 7. The stop-band SL array FSS element parameters, with
the dielectric substrate shown in green and the conductor (copper) in brown [19]

The dimensions of the SL FSS unit cell are as follows (all in mm): $p = 1.4$, $d = 1.2$, $g = 0.2$, and $s = 0.1$ [21]. Figure 8 illustrates the proposed configurations for a tuneable rectangular MPA with FSSs. Three layouts have been used: (1) The tuneable rectangular MPA. (2) Stop-band SL array FSS used as a ground plane to reflect the plane wave in phase. (3) Pass-band SL mech-patch array FSS used as a superstrate to reduce surface waves. A pass-band SL mech-patch array FSS can be realised by using the Babinet duals in Figure 7. Provided that the structure is symmetrical, Babinet's principle can be employed to change from a stop-band SL array FSS to a pass-band SL mech-patch array FSS, where the conductive and non-conductive spaces are reversed [22].

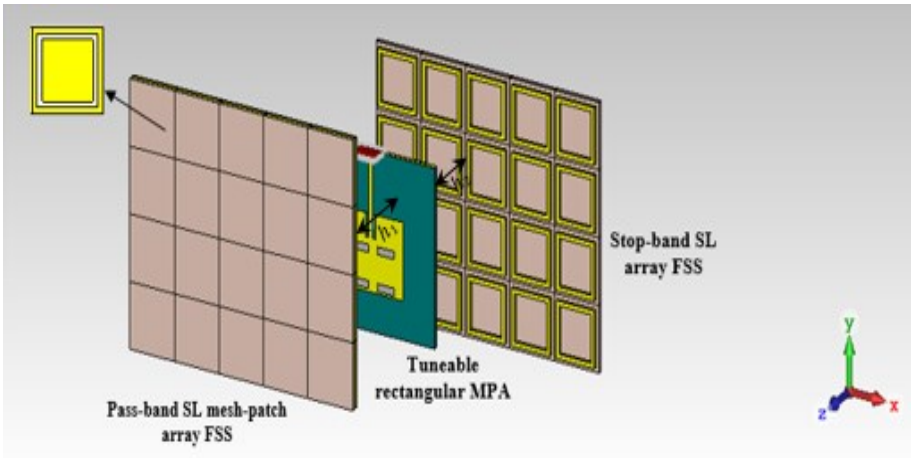

Figure 8. A tuneable rectangular MPA between two FSSs

The resonant height of the FSS superstrate antenna is predicted with the help of resonance estimation, using the standard raytracing technique. The resonance condition for the antenna structure at the boresight angle and the operating frequency as a function of the height of the superstrate above/below the substrate are obtained as [23]:

$$h = \frac{N\lambda_o}{2} + \left(\frac{\varphi_{\Gamma(ground,sub,air\ gap)} + \varphi_{FSS}}{\pi}\right)\frac{\lambda_o}{4} \quad \text{for} \quad N = 1,2,3, \ldots \ldots \tag{18}$$

where N is an integer, λ_o is the free-space wavelength, $\varphi_{\Gamma(ground,sub,air\ gap)}$ is the reflection phase angle of the ground plane, and φ_{FSS} is the reflection phase angle of the superstrate unit cell. The value of $\varphi_{\Gamma(ground,sub,air\ gap)}$ is obtained from (19);

$$\varphi_{\Gamma(ground,sub,air\ gap)} = \pi - 2\tan^{-1}\left(\frac{Z_d \tan(\beta d)}{Z_o}\right) \tag{19}$$

where $Z_d = (Z_o/\sqrt{\varepsilon_r})$ is the characteristic impedance of the wave in the dielectric substrate, Z_o is the characteristic impedance of the wave in free space, and $\beta = \left(\frac{2\pi\sqrt{\varepsilon_r}}{\lambda_o}\right)$ is the phase constant of the wave in the substrate. An expression for estimating the boresight directivity, relative to that of the primary antenna (feed antenna) has been derived in [24]

$$D = \frac{1+|\Gamma_{FSS}(f_r,\theta=0)|}{1+|\Gamma_{FSS}(f_r,\theta=0)|} \quad (20)$$

It can be seen from (20) that the directivity of the rectangular MPA increases as the magnitude of the reflection coefficient increases. Thus, in order to have a perfect FSS superstrate, the requirements of a flat reflection phase and a high reflection magnitude versus frequency must be satisfied [25]. At 60 GHz, the FSS reflection coefficient is 0.8 and the corresponding relative directivity is estimated to be about 9.5 dBi. Therefore, when the primary source antenna has 5 to 7 dBi gain (such as a rectangular MPA), placing this FSS superstrate at an appropriate distance above/below the ground plane can increase the gain to as much as 14 dBi. Interestingly, this estimated gain is in good agreement with the prediction of the CST-MWS model. The various parameters in (18) and (19) are summarised in Table 6. For the proposed configuration, the gap was varied to obtain the optimum distance between the MPA and FSS. The ideal gaps for a single rectangular MPA were found to be 2 and 2.2 mm for h_1 and h_2, respectively, as shown in Figure 8.

Table 6. Parameter Values of (18 and 19)

$f_r\ (GHz)$	$Z_o\ (\Omega)$	ε_r	N	$\beta\ (mm^{-1})$	$d\ (mm)$
60	377	2.2	1	1.86	0.1
$\boldsymbol{Z_d}\ (\Omega)$	$\boldsymbol{\varphi_{\Gamma(ground,sub,air\ gap)}}$	$\boldsymbol{\varphi_{FSS\ pass-band}}$	$\boldsymbol{\varphi_{FSS\ stop-band}}$	$\boldsymbol{h_1\ (mm)}$	$\boldsymbol{h_2\ (mm)}$
254.17	165.6^o	-167	-166	1.95	2.3

5. RESULTS AND DISCUSSION

In this section, the results obtained from the antenna simulation in the CST-MWS simulation software are illustrated. The simulated return loss (S_{11}) for the tuneable rectangular MPA in the ON and OFF states from the time domain solver of CST-MWS is presented in Figure 9. In general, the MPAs have poor gain; this is because the antenna gain is proportional to h and inversely proportional to ε_r [23]. Figure 10 shows the three-dimensional results for the far field of the tuneable rectangular MPA at the operating frequencies f_r= 52.35, 59.3, 59.89, and 60 GHz, both with and without FSSs. The antenna has a reasonable gain in this operating frequency band; however, by using FSSs the antenna parameters are enhanced, where gain is significantly increased from 5.7 to 12.1 dBi, bandwith increased from 2.3334 to 3.18 GHz, and the S_{11} decreased from -42.4 to -54 dB at the highest value of f_r (60 GHz).

A single main lobe of a reasonable beam width characterises the radiation pattern. In the azimuthal and elevation planes, the beam widths are often identical, resulting in a relatively circular beam, although this is by no means universal. The beam widths can be manipulated to produce an antenna with higher or lower gain, depending on the required application. Figure 11 illustrates the 3-dB beam width for the proposed antenna at various operating frequency bands. The bandwidth is calculated from the return loss plot at S_{11}=-10 dB. A summary of the results and the bandwidths are illustrated in Table 7.

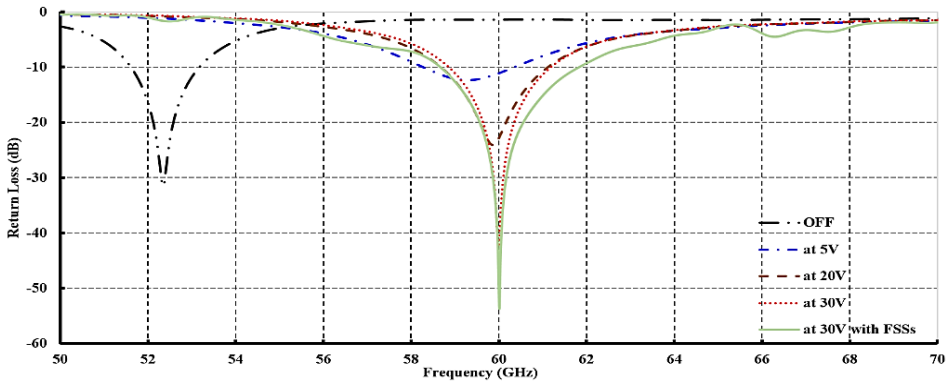

Figure 9. S_{11} versus frequency for various values of the applied voltage V_B

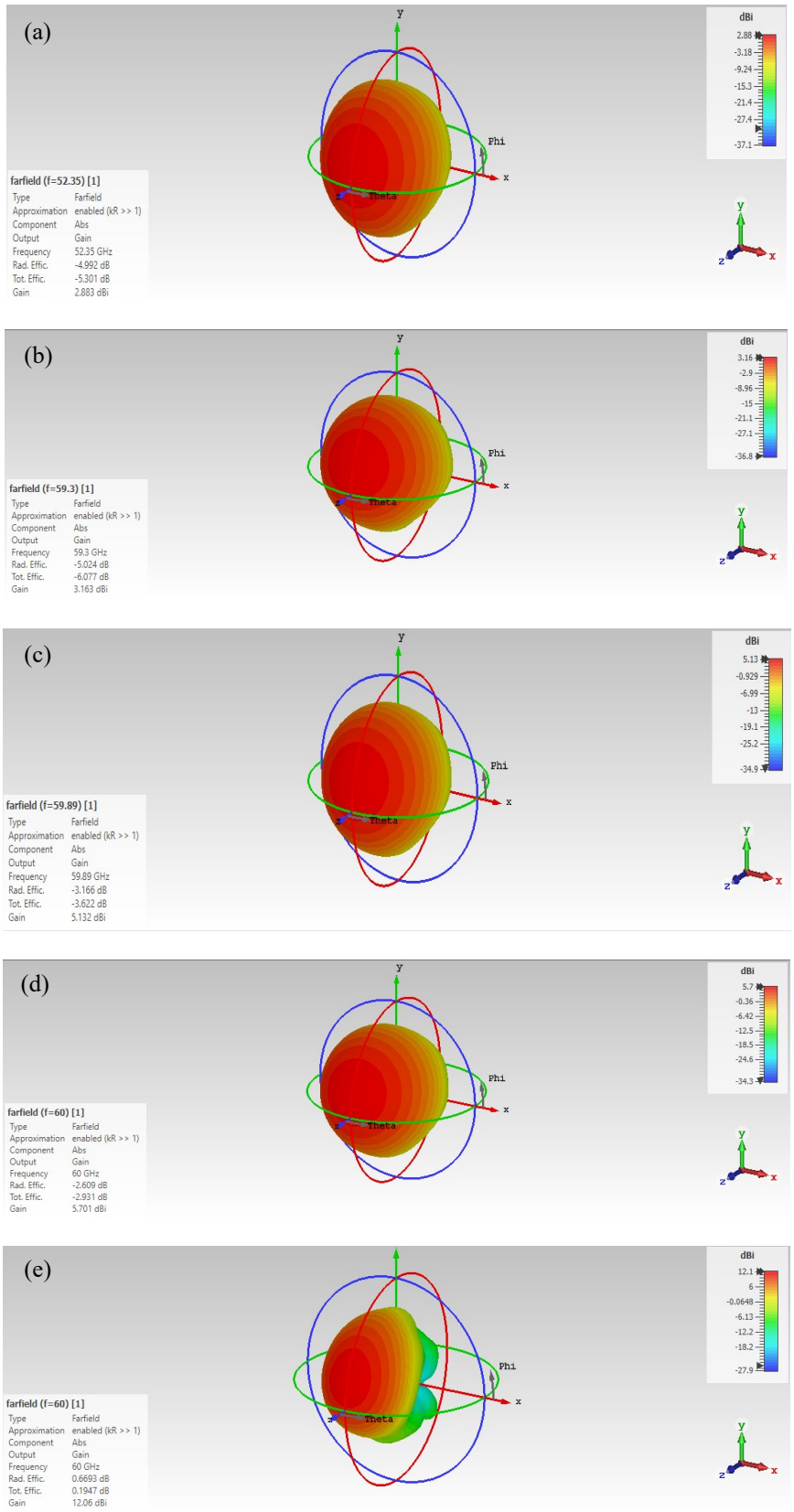

Figure 10. Far field simulation results for the proposed tuneable rectangular MPA; (a) f_r=52.35 GHz at $V_B=$ 0.5 V, (b) f_r=59.3 GHz at $V_B=$5 V, (c) f_r=59.89 GHz at $V_B=$ 20 V, (d) f_r=60 GHz at $V_B=$ 30 V, and (e) f_r=60 GHz at $V_B=$ 30 V with FSSs

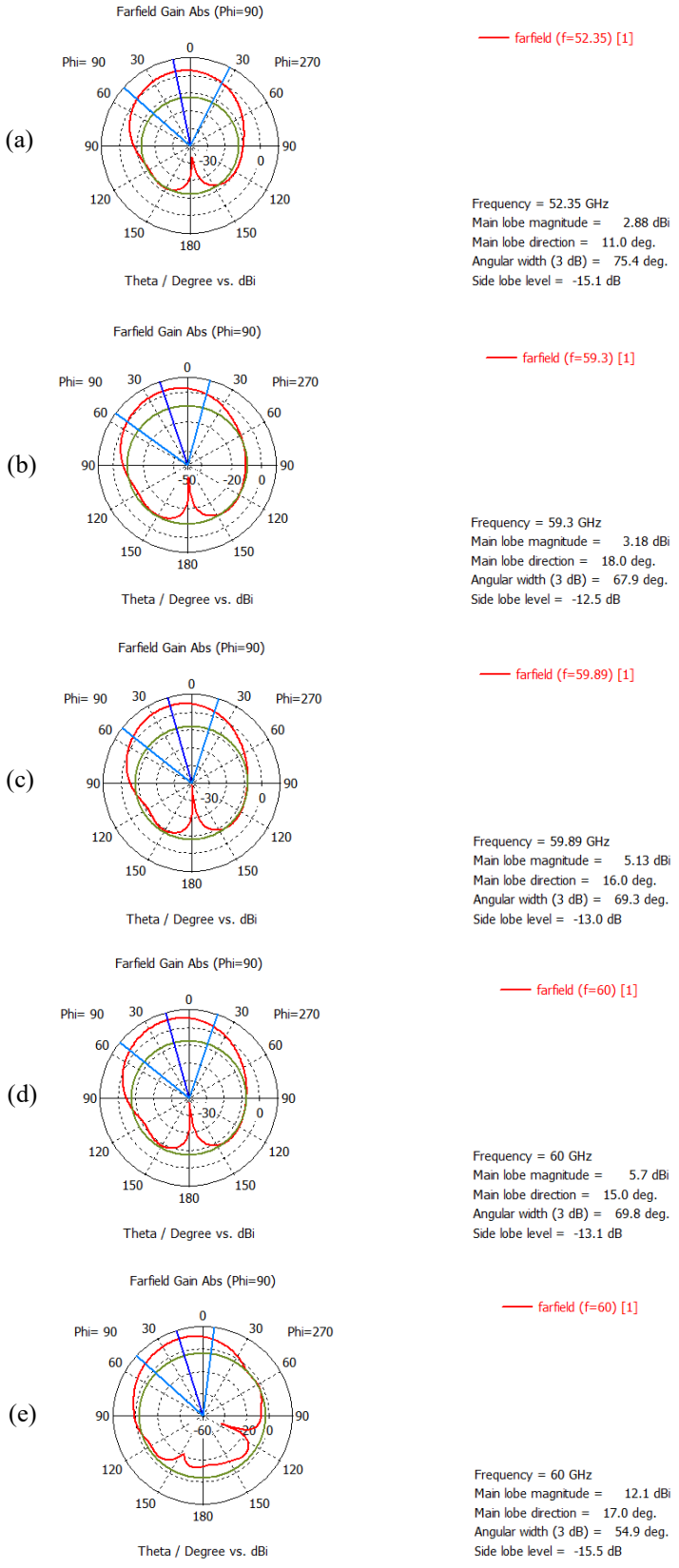

Figure 11. Radiation pattern produced by the MPA; (a) f_r=52.35 GHz at $V_B=$ 0.5 V, (b) f_r=59.3 GHz at $V_B=$5 V, (c) f_r=59.89 GHz at $V_B=$ 20 V, (d) f_r=60 GHz at $V_B=$ 30 V, and (e) f_r=60 GHz at $V_B=$ 30 V with FSSs

Table 7. Summary of results for the proposed tuneable rectangular MPA

	Without FSS				With FSS
Applied V_B(V)	0.5 (OFF)	5	20	30	30
f_r (GHz)	52.35	59.3	59.89	60	60
Bandwidth (GHz)	1.559	2.0788	2.4447	2.3334	3.18
S_{11} (dB)	-31.2	-12.35	-24	-42.4	-54
Gain (dBi)	2.88	3.16	5.13	5.7	12.1

6. CONCLUSION

A novel hybrid graphene-metal tuneable antenna has been presented in this paper. Tunability was obtained by placing graphene strips inside the antenna radiating patch, which alter the current propagation on the surface of the antenna radiating patch. The proposed tuneable rectangular MPA had a reasonable gain with many resonance frequencies in the range of 52.53 to 60 GHz, which depended on the V_B applied to the graphene strips. When V_B was increased, the surface impedance of the graphene strips decreased, which shifted the resonance frequency upward and broadens the antenna bandwidth. The results of a comparison between designs with and without FSSs demonstrated that the gain, return loss, and bandwidth have been improved significantly by incorporating an FSSs.

REFERENCES

[1] A. Gupta, S. Member, R. K. Jha, and S. Member, "A Survey of 5G Network : Architecture and Emerging Technologies," *IEEE Access*, vol. 3, pp. 1206-1232, 2015.

[2] T. H. Jang, et al., "A Wideband Aperture Efficient 60-GHz Series-Fed E-shaped Patch Antenna Array with Co-polarized Parasitic Patches," *IEEE Trans. Antennas Propag.*, vol. 64, no. 12, pp. 1-4, 2016.

[3] F. Azam, S. Bashir, and M. A. Sohaib, "Millimeter Waves Frequency Reconfigurable Antenna for 5G Networks," *Mehran Univ. Res. J. Eng. Technol.*, vol. 619, no. 3, pp. 619-626, 2019.

[4] M. Salarpour, F. Farzaneh, S. Member, and R. B. Staszewski, "A Low Cost-Low Loss Broadband Integration of a CMOS Transmitter and Its Antenna for mm-Wave FMCW Radar Applications," *AEUE - Int. J. Electron. Commun.*, vol. 95, pp. 313-325, 2018.

[5] A. Farahbakhsh, A. U. Zaman, and P. Kildal, "Design and Fabrication of A High - Gain 60 GHz Corrugated Slot Antenna Array with Ridge Gap Waveguide Distribution Layer," *IEEE Trans. Antennas Propag.*, vol. 64, no. 7, pp. 2905-2913, 2016.

[6] M. N. Hindia, T. A. Rahman, and T. M. Yazdani, "Outdoor large-scale path loss characterization in an urban environment at 26, 28, 36, and 38 GHz," *Phys. Commun.*, vol. 27, pp. 150-160, 2018.

[7] T. Singh, K. A. Ali, H. Chaudhary, D. R. Phalswal, and V. Gahlaut, "Design and Analysis of Reconfigurable Microstrip Antenna for Cognitive Radio Applications," *Wirel. Pers. Commun.*, vol. 98, no. 2, pp. 2163–2185, 2017.

[8] K. Rouhi, H. Rajabalipanah, and A. Abdolali, "Multi-bit graphene-based bias-encoded metasurfaces for real-time terahertz wavefront shaping: From controllable orbital angular momentum generation toward arbitrary beam tailoring," *Carbon N. Y.*, vol. 149, pp. 125-138, 2019.

[9] H. Chen, Z. Liu, and W. Lu, "Microwave Beam Reconfiguration Based on Graphene Ribbon," *IEEE Trans. Antennas Propag.*, vol. 66, no. 11, pp. 6049-6056, 2018.

[10] H. A. Abdulnabi and Y. Y. Al-aboosi, "Design of Tunable Multiband Hybrid Graphene Metal Antenna in Microwave Regime," *Indones. J. Electr. Eng. Comput. Sci.*, vol. 12, no. 3, pp. 1003-1009, 2018.

[11] E. Dheyab and N. Qasem, "Design and Optimization of Rectangular Microstrip Patch Array Antenna Using Frequency Selective Surfaces for 60 GHz," *Int. J. Appl. Eng. Res.*, vol. 11, no. 7, pp. 4679-4687, 2016.

[12] N. Qasem, "Enhancing the Capacity of the Indoor 60 GHz Band Via Modified Indoor Environments Using Ring Frequency Selective Surface Wallpapers and Path Loss Models," *Int. J. Electr. Comput. Eng.*, vol. 8, no. 5, pp. 3003-3020, 2018.

[13] M. Ibrahimy and S. Motakabber, "Microstrip patch antenna with defected ground structure for biomedical application," *Bull. Electr. Eng. Informatics*, vol. 8, no. 2, pp. 586–595, 2019.

[14] B. S. Taha, H. M. Marhoon, and A. A. Naser, "Simulating of RF energy harvesting micro-strip patch antenna over 245 GHZ," *International Journal of Engineering and Technology*, vol. 7, no. 4, pp. 5484-5488, 2018.

[15] S. Islam, M. I. Ibrahimy, S. Motakabber, and Z. Hossain, "A Rectangular Inset-Fed Patch Antenna with Defected Ground Structure for A Rectangular Inset-Fed Patch Antenna with Defected Ground Structure for ISM Band," in *7th International Conference on Computer and Communication Engineering (ICCCE), IEEE*, pp. 104-108, 2018.

[16] M. Yasir, et al., "A Planar Antenna with Voltage-Controlled Frequency Tuning Based on Few-Layer Graphene," *IEEE Antennas Wirel. Propag. Lett.*, vol. 16, pp. 2380–2383, 2017.

[17] C. Nu, R. Cheung, S. Member, and S. John, "Performance Analysis Of Hybrid Metal-Graphene Frequency Reconfigurable Antennas In The Microwave Regime," *IEEE Trans. Antennas Propag.*, vol. 65, pp. 1558-1569, 2017.

[18] A. Hlali, Z. Houaneb, and H. Zairi, "Dual-Band Reconfigurable Graphene-Based Patch Antenna in Terahertz Band : Design , Analysis and Modeling Using WCIP Method," *Prog. Electromagn. Res. C*, vol. 87, pp. 213-226, 2018.

[19] H. A. Abdulnabi, M. A. Shuriji, S. Ahmed, and H. A. Abdulnabi, "UWB THz plasmonic microstrip antenna based on graphene," *TELKOMNIKA Telecommunication Computing Electronics Control*, vol. 18, no. 1, pp. 30-36, 2020.

[20] N. Qasem and R. Seager, "Indoor Band Pass Frequency Selective Wall Paper Equivalent Circuit & Ways to Enhance Wireless Signal," in *2011 Loughborough Antennas & Propagation Conference*, pp. 1-4, 2011.
[21] N. Qasem, E. A. Aldorgam, and H. Y. Alzou'bi, "Overcoming the Influence of Human Shadowing and Obstacles via Modified Building Using Frequency Selective Wallpapers for 60 GHz," *J. Commun. Comput.*, vol. 13, no. 2, pp. 90-101, 2016.
[22] N. Qasem, "Enhancing wireless communication system performance through modified indoor environments," *Loughborough University*, 2014.
[23] A. Foroozesh and L. Shafai, "Investigation Into the Effects of the Patch-Type FSS Superstrate on the High-Gain Cavity Resonance Antenna Design," *IEEE Trans. Antennas Propag.*, vol. 58, no. 2, pp. 258-270, 2010.
[24] A. P. Feresidis and J. C. Vardaxoglou, "High gain planar antenna using optimised partially reflective surfaces," *IEEE Proc-Microiv. Antennas Propuq.*, vol. 148, no. 6, pp. 345-350, 2001.
[25] R. G. Mishra, E. Studies, G. Chathuranga, R. Mishra, and E. Studies, "Analysis of the Relationship Between Substrate Properties and Patch Dimensions in Rectangular-Shaped Microstrip Antennas," in *In Intelligent Communication, Control and Devices Springer, Singapore*, pp. 65-72, 2018.

BIOGRAPHIES OF AUTHORS

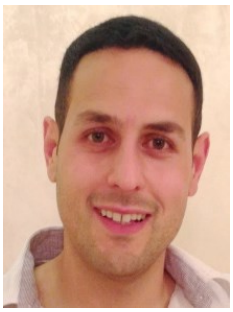

Nidal Qasem received his B.Sc. degree in Electronics and Communications Engineering (Honours) from Al-Ahliyya Amman University, Amman, Jordan, in 2004. He obtained his M.Sc. degree in Digital Communication Systems for Networks & Mobile Applications (DSC) in 2006, followed by a Ph.D. in Wireless and Digital Communication Systems, both from Loughborough University, Loughborough, United Kingdom. He currently holds the position of associate professor in the department of Electronics and Communications Engineering at Al-Ahliyya Amman University. His research interests include propagation control in buildings, specifically improving the received power, FSS measurements and designs, antennas, ultra-wide band, orbital angular momentum, and wireless system performance analyses. He is a senior member of the IEEE.

Hamzah M. Marhoon received his B.Sc. degree in Electrical Engineering (Rank 2) from College of Engineering Al-Mustansiriyah University, Baghdad, Iraq in 2016. He obtained his M.Sc. degree in Communications Engineering in 2020 from Al-Ahliyya Amman University, Hashemite Kingdom of Jordan. He works as a teaching assistant at Al-Esraa University College, Baghdad, Iraq. His research interests include Antennas, Tuneable Antennas, IoT, Energy Harvesting Antennas, and Embedded Systems.
https://orcid.org/0000-0001-5613-6685.